Available online at www.sciencedirect.com
SCIENCE DIRECT®
Scripta Materialia 51 (2004) 571–575
Scripta MATERIALIA
www.actamat-journals.com

Measurements and predictions of strain pole figures for uniaxially compressed stainless steel

C. Larsson [a,*], B. Clausen [b], T.M. Holden [b], M.A.M. Bourke [b]

[a] Division of Engineering Materials, Department of Mechanical Engineering, Linköping University, 58183 Linköping, Sweden
[b] Los Alamos National Laboratory, Los Alamos, NM 87545, USA

Received 7 December 2003; received in revised form 4 May 2004; accepted 19 May 2004
Available online 17 June 2004

Abstract

Strain pole figures representative of residual intergranular strains were determined from an −2.98% uniaxially compressed austenitic stainless steel sample. The measurements were made using neutron diffraction on the recently commissioned Spectrometer for Materials Research at Temperature and Stress (SMARTS) at Los Alamos National Laboratory, USA. The measurements were compared with predictions from an elasto-plastic self-consistent model and found to be in good agreement.
Published by Elsevier Ltd. on behalf of Acta Materialia Inc.

Keywords: Neutron diffraction; Modeling; Strain pole figure; Plastic deformation; Stainless steel

1. Introduction

Single-phase engineering materials are inhomogeneous at the scale of the grain size, since the grains generally have different elastic and plastic properties depending on their crystallographic orientation. Accordingly, the orientation of an individual grain with respect to the loading direction and its particular properties determine the magnitude of the strain in it. For applied loads, significantly less than the macroscopic yield stress, grains in a polycrystal deform elastically and the associated strains disappear after unloading. However, when the applied load approaches macroscopic yield, plasticity initiates in grains with favorably oriented slip systems causing a redistribution of the already heterogeneous strain field. The elastic strains that develop in the grains to accommodate plastic deformation localized within the microstructure are termed intergranular strains (or Type-II strains) [1]. Intergranular strains remain in the grains after unloading and can conveniently be measured by neutron diffraction [2]. Strains measured in a neutron measurement record a superposition of intergranular strains and strains on a larger scale called macrostrains (Type-I) [1]. Where the principle interest is macrostrain, it is necessary to account first for the intergranular contribution, which is a major motivation of this study. Presuming measurements are made with sufficient coverage, strain pole figures from neutron measurements can represent the strains, in respect to the deformation axis, in grains as a function of their crystallographic orientation.

An elasto-plastic self-consistent (EPSC) approach [3] can predict residual intergranular strains in polycrystals. Residual intergranular strains in the same austenitic stainless steel as in this study have been determined with neutron diffraction and compared to such a model during uniaxial tensile loading [4] and during cyclic loading [5]. However, that work was limited to strain measurements in two directions. Calculated and measured strain pole figures from four reflections have also been

* Corresponding author. Tel./fax: +1-407-672-5724.
E-mail address: clarsson@cfl.rr.com (C. Larsson).

1359-6462/$ - see front matter Published by Elsevier Ltd. on behalf of Acta Materialia Inc.
doi:10.1016/j.scriptamat.2004.05.030

presented for an Inconel-600 alloy after uniaxial plastic deformation in both compression and tension [6].

In this study, time-of-flight neutron diffraction enabled the simultaneous recording of multiple lattice plane hkl reflections in individual spectra for a given sample orientation and was employed to determine strain pole figures. The sample was an austenitic stainless steel cube that was uniaxially compressed to −2.98% plastic strain. The resulting strain pole figures for eight lattice plane hkl reflections were obtained by performing measurements in a series of orientations by using an Euler cradle. The results were compared with predictions from an elasto-plastic self-consistent model. The objectives were twofold: first, to validate an elasto-plastic self-consistent approach in predicting intergranular strains, and second, to demonstrate the capability of a recently commissioned third generation time-of-flight neutron diffractometer—Spectrometer for Materials Research at Temperature and Stress (SMARTS) [7] at Los Alamos National Laboratory to obtain strain pole figures representative of residual intergranular strains.

2. Sample preparation

The austenitic stainless steel had a nominal composition (wt%) of 62.73 Fe, 18.25 Cr, 13.42 Ni, 3.66 Mo, 1.48 Mn, 0.44 Si and 0.02 C. The material was received in the form of a rolled plate, had a relatively weak texture (a maximum of 1.6 × random) and an average grain size of 28 μm. The initial texture for this material has previously been investigated and the orientation distribution function (ODF) reported in Ref. [4]. Two $10\times10\times10$ mm^3 cubic samples were electrical discharge machined from the rolled plate. The cube sides were parallel to the rolling direction. One cube was uniaxially compressed to −2.98% in a direction normal to the rolling and transverse directions and the other was used, in the undeformed state, as a reference sample.

3. Elasto-plastic self-consistent model

An EPSC model was used to predict the measured strains. In this model, each grain in the sample is treated as an elasto-plastic spherical inclusion in an elasto-plastic homogeneous matrix whose properties are the average of all the grains in the polycrystal. This model is more sophisticated than other models such as Sachs and Taylor since it incorporates interaction between matrix and inclusion [8]. While a finite element approach (when compared to an EPSC model) can provide additional detail by including interactions between grains [9], such an approach is not necessary for direct comparison with neutron diffraction measurements, which average over many grains. The constraints imposed on the self-consistent model are that the average of the stress and the strain rates of all the modeled grains are equal to the overall stress and strain rates of the sample. During plastic deformation, the type and number of slip systems that are activated in each grain are calculated. In fcc stainless steel the possible slip systems are the $\{1\,1\,1\}\langle1\,1\,0\rangle$ systems. For a more detailed description of the EPSC model, see Refs. [3,4,8]. In the present calculations we used the model presented in Ref. [3], which uses a slightly different hardening law from that in Ref. [4]. However, we have obtained the same good agreement between the calculated and measured macroscopic stress–strain curve, Fig. 1a, as reported in Ref. [4]. The critical resolved shear stress is the stress required to move a dislocation through the lattice and the hardening parameters describe the evolution of this stress with plastic deformation, which is determined from the macroscopic stress–strain curve. The hardening parameters for the Voce type hardening law used in the current EPSC model are explained in detail in Ref. [10] and shown graphically in Fig. 1b. The hardening parameters were $\tau_0=87.0$ MPa, $\tau_1=8.0$ MPa, $\theta_0=1000$ MPa and $\theta_1=340$ MPa. The material parameters for stainless steel were obtained from Ref. [4]. 23,000 grains were incorporated in this model.

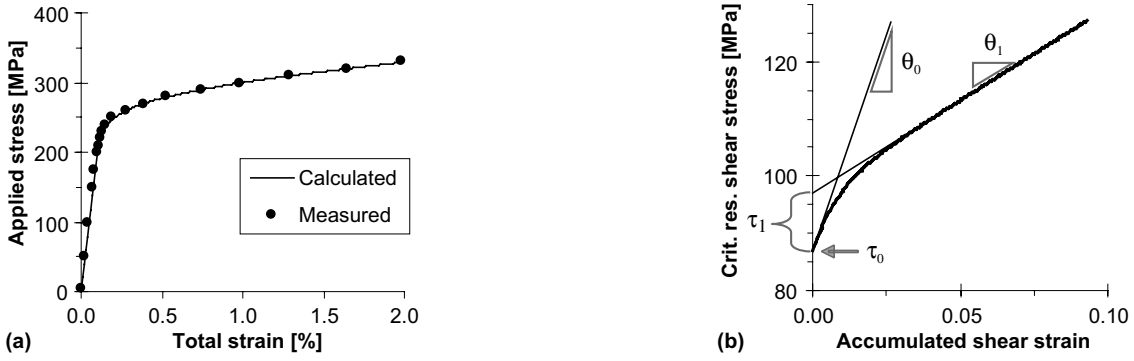

Fig. 1. (a) Measured and calculated macroscopic stress–strain curve. (b) Graphical representation of the hardening parameters used in the EPSC model.

4. Neutron diffraction technique

The Spectrometer for Materials Research at Temperature and Stress at the Los Alamos Neutron Science Center at Los Alamos National Laboratory was used to determine the residual intergranular strains. The incident neutron beam was defined by 18 mm wide and 18 mm high boron nitride apertures that were placed 100 mm from the sample. The detector bank, at +90°, spanned ±13° in the horizontal plane and ±15° in the vertical plane. As shown in Fig. 2a, the sample was held in a remote controlled Euler cradle that facilitated rotation in χ and φ directions, and the cradle in turn was placed on a computer-controlled xyz–θ stage. The sample was positioned with the aid of two Leica theodolites that, by triangulation, located a sample with respect to the center of the spectrometer to better than an accuracy of 0.1 mm. It was aligned with the rolling direction parallel to the scattering vector at $\chi=0$ and $\varphi=0$ (see Fig. 2b). Spectra were measured at every 10° intervals in the φ direction and at 15° intervals in the χ direction. A total of 70 spectra were measured in both the reference sample and in the uniaxially compressed sample.

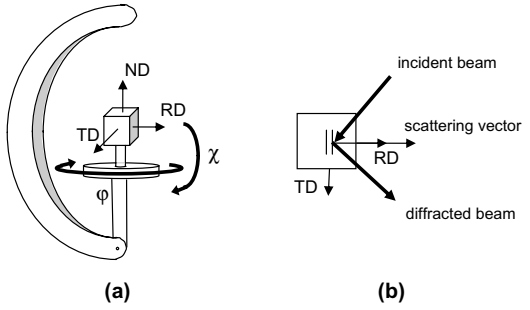

Fig. 2. (a) Schematic of the Euler cradle setup in which the samples were rotated in φ and χ directions to obtain strain pole figures. The rolling direction (RD), normal direction (ND) and transverse direction (TD) are indicated. (b) Plan top view of a sample for values of $\chi=0$ and $\varphi=0$ where the scattering vector is parallel to the rolling direction.

Each spectrum took about 10 min to record at a beam current of 100 μA.

5. Results and discussion

The time-of-flight technique at a pulsed source facilitates the recording of entire spectra for a given sample orientation. Analyses of the spectra were made using a GSAS [11] subroutine RAWPLOT and the 111, 200, 220, 311, 331, 420, 422 and 531 reflections were fitted in each spectrum to determine the respective d-spacings. For a given χ and φ angle, a strain ε^{hkl} was calculated from

$$\varepsilon^{hkl}=\frac{d^{hkl}-d_0^{hkl}}{d_0^{hkl}}, \tag{1}$$

where d^{hkl} is the hkl d-spacing in the plastically deformed sample and $d_0{}^{hkl}$ is the corresponding hkl d-spacing in the undeformed reference sample at the same χ and φ position in the beam. Strain pole figures were subsequently constructed by incorporating the calculated strains from Eq. (1) for various χ and φ angles. The use of the undeformed reference sample in Eq. (1) implies that the reported strains correspond to elastic intergranular strains associated with the plastic deformation and do not include possible contributions from previously existing strains. It also corrects for possible physical shifts of the sample in the beam upon rotation that can lead to spurious shifts in apparent strain as demonstrated by Wang et al. [12].

Strain pole figures for the compressed sample were measured and calculated for the 111, 200, 220, 311, 331, 420, 422 and 531 reflections. The largest variations were observed for the 200 reflection which is shown in Fig. 3. Large compressive strains at low and high χ angles (i.e., near the normal direction and along the rolling direction—transverse direction locus on the perimeter of the pole figure), with tensile strains at intermediate χ angles, are seen in both measurement (Fig. 3a)

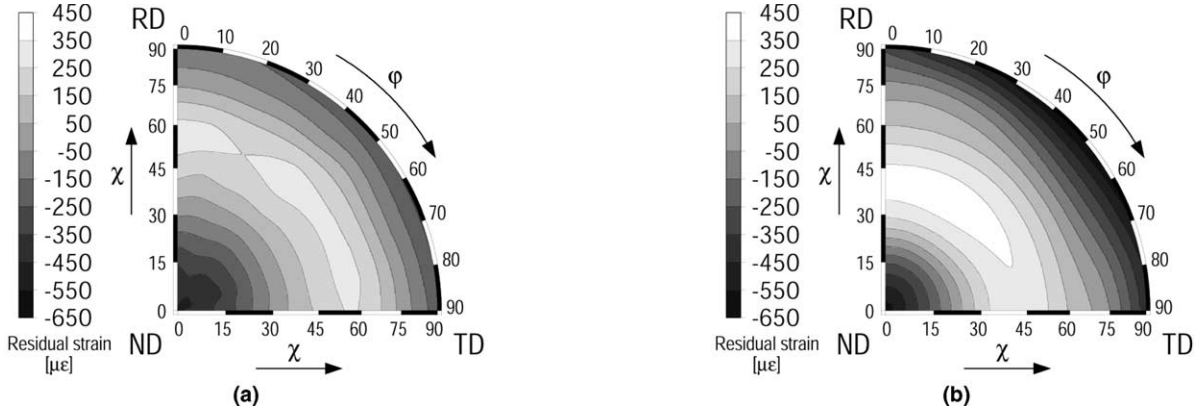

Fig. 3. 200 strain pole figures from (a) neutron diffraction measurements and (b) calculations from an elasto-plastic self-consistent model.

and model (Fig. 3b). However, larger strain minimum and maximum were seen in the model. The strain maximum was seen at $\chi = 40°$ in the model as opposed to $\chi = 55°$ in the measurement.

Only small strain differences were observed as a function of φ (i.e., around the compression axis) in Fig. 3, and therefore the results for all the reflections were averaged in the φ direction and presented as graphs of strain vs. χ in Fig. 4, for easier comparisons between measurements and model. The error bars in Fig. 4 have contributions from the uncertainties in the deformed and undeformed peak positions. The modeled strains are within the error of the measured strains, except for the 200 reflection that is affected by the aforementioned shift in maximum value to a lower χ for the model.

Three trends are observed; one convex-up, e.g., 200, one concave-down, e.g., 220, and one that is slightly positive at small χ angles and fairly flat at high χ angles, e.g., 422. The largest measured residual intergranular strain variation with χ is found in the 200 reflection while the 420 reflection shows the smallest strain variation. An attempt to analytically justify these observations is not straightforward because of the difficulty to separate contributions from elastic anisotropy and strain redistribution due to slip along preferred crystallographic systems. Hence the recourse to predictions from a comprehensive EPSC model that in this case has agreed reasonably well with measurements.

Using the validated model, the influence of texture on the residual intergranular strains for the deformed sample was studied by calculating strain pole figures for (i) a random set of grains (ii) a set of grains representing the weak initial texture in the sample (i.e., maximum of 1.6 × random) and (iii) a set of grains representing a stronger texture (i.e., maximum of 6 × random). Fig. 5 shows the calculated strain pole figures for the 311 reflection using the random, and the strong and weak textured sets of grains. When considering strain values averaged over φ, the largest difference among all measured hkl reflections was seen in the 311 reflection. The difference is only 150 microstrain between the random and the 6 × random texture at $\chi = 90$, with the effect of texture being minimal over most of the range of χ angles. A comparison of the random sample with the 1.6 × random texture showed that the differences are always less than 55 microstrain for all hkl reflections, as would be expected from the very weak initial rolling texture. However, when studying rotational symmetry, i.e., φ depend-

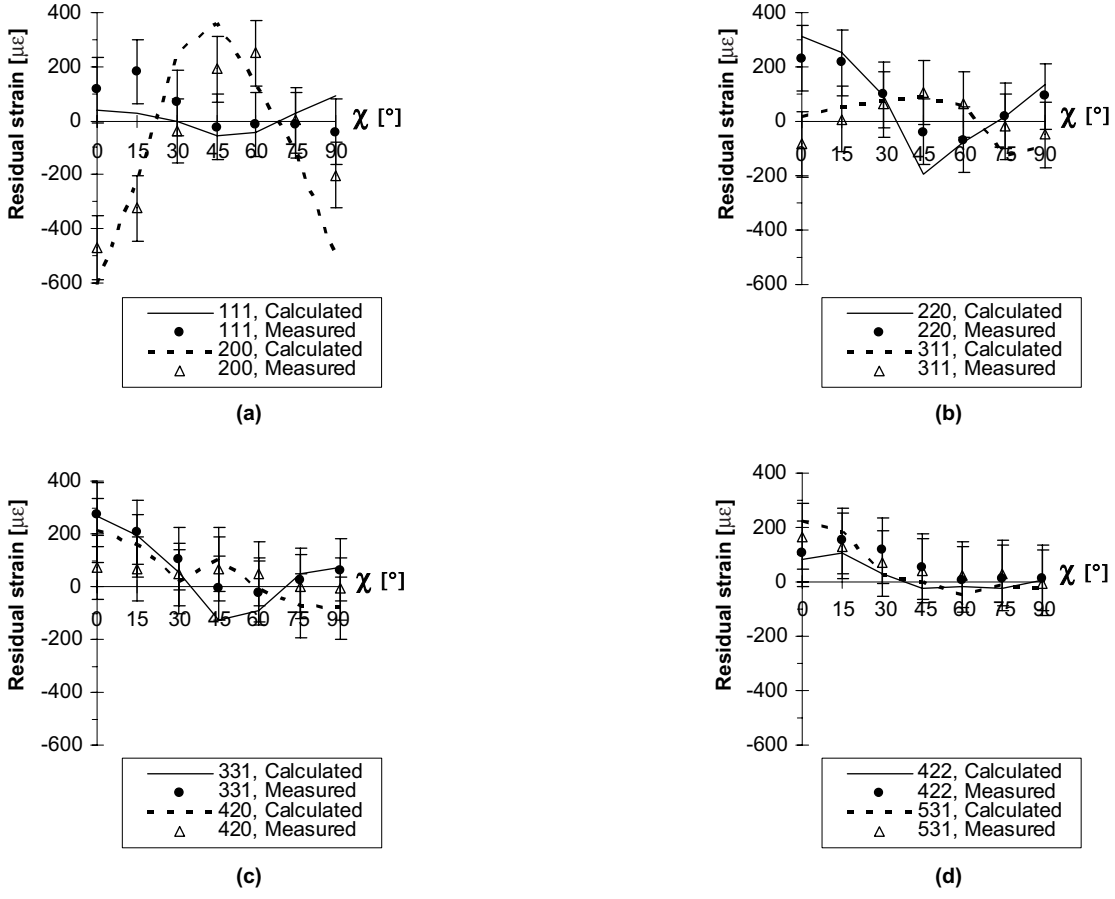

Fig. 4. Calculated and measured strains vs. χ (averaged along φ) for (a) 111, 200; (b) 220, 311; (c) 331, 420; and (d) 422, 531 reflections.

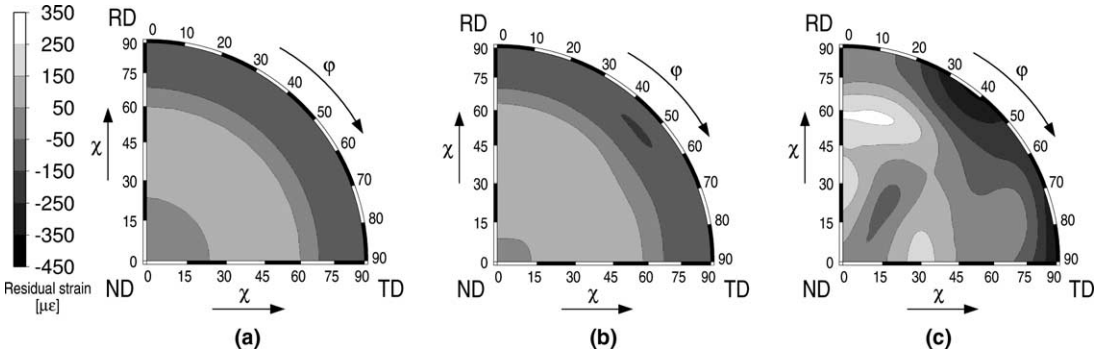

Fig. 5. Calculated strain pole figures for the 311 reflection using (a) a random set of grains, (b) the sample's initial texture (i.e., maximum of 1.6 × random) and (c) an arbitrarily selected stronger texture (i.e., maximum of 6 × random).

ence of the strain for the same χ, larger differences were seen as illustrated by Fig. 5. It was noted that results from the prediction of the random set of grains (Fig. 5a) had full rotational symmetry, while some φ dependence of the strain for the same χ was noted for the 1.6 × random textured sample (Fig. 5b). For both the prediction and the measurements in the 1.6 × random textured sample, the maximum variation of the strain with φ (in any of the hkl directions at the same χ) was 130 microstrain. On the other hand, the calculation with 6 × random texture (Fig. 5c) showed large φ dependence of the strain (up to 900 microstrain for the 200 reflection) at the same χ. Thus averaging over φ (as done here) without introducing a large error is only recommended when the material is weakly textured.

6. Conclusions

Measured strain pole figures were in reasonable agreement with residual intergranular strain calculations from an elasto-plastic self-consistent model. The average of the differences between measurement and model for the angles and reflections considered was 17 microstrain, well within the error of 150 microstrain attributed to the measurement technique. The largest measured residual strain variation with χ, 700 microstrain, was found for the 200 reflection and the 420 reflection showed the smallest strain variation of 100 microstrain. Using the model, the effect of a stronger (6 × random) initial texture was considered. Thus, while the measured sample's 1.6 × random texture did not show significant effects, the predictions for the stronger texture reduced the inherent rotational symmetry of the strain field with strain variations of up to 900 microstrain. This work additionally demonstrated the capability of the spectrometer (SMARTS) at Los Alamos National Laboratory to rapidly (≈10 min in steel with a neutron beam current of 100 μA) acquire spectra for determining strain pole figures from a sample in a computer-controlled Euler cradle.

Acknowledgments

The authors are grateful to T. Ericsson and S. Vogel for useful discussions. CL acknowledges financial support from the Sweden–America Foundation and the Hans Werthén Fund from the Royal Swedish Academy of Engineering Sciences. Los Alamos Neutron Science Center is a national user facility funded by the United States Department of Energy, Office of Basic Energy Sciences, under contract number W-7405-ENG-36.

References

[1] Macherauch E, Kloos KH. In: Macherauch E, Hauk V, editors. Residual stresses in science and technology. DGM Informationsgesellschaft Oberursel; 1987. p. 3.
[2] Hutchings MT, Krawitz AD, editors. Measurement of residual and applied stress using neutron diffraction. NATO ASI Series E No 216. The Netherlands: Kluwer; 1992.
[3] Turner PA, Tomé CN. Acta Metall Mater 1994;42:4143.
[4] Clausen B, Lorentzen T, Bourke MAM, Daymond MR. Mater Sci Eng A 1999;259:17.
[5] Lorentzen T, Daymond MR, Clausen B, Tomé CN. Acta Mater 2002;50:1627.
[6] Holden TM, Holt RA, Tomé CN. Mater Sci Eng A 2000;282:131.
[7] Bourke MAM, Dunand DC, Ustundag E. Appl Phys A: Mater Sci Process 2002;74(6):1707.
[8] Clausen B, Lorentzen T, Leffers T. Acta Mater 1998;46(9):3087.
[9] Dawson P, Boyce D, MacEwen S, Rogge R. Metall Mater Trans A 2000;31:1543.
[10] Tomé CN, Maudlin PJ, Lebensohn RA, Kaschner GC. Acta Mater 2001;49:3085.
[11] Larson AC, Von Dreele RB. General structure analysis system (GSAS). Los Alamos Report No. LAUR 8-748. Los Alamos: Los Alamos National Laboratory; 1986.
[12] Wang X-L, Wang YD, Richardson JW. J Appl Cryst 2002;35:533.